J|A|C|S
COMMUNICATIONS

Published on Web 10/11/2006

A Simple Method for Kinetic Control of DNA-Induced Nanoparticle Assembly

Mathew M. Maye,[†] Dmytro Nykypanchuk,[†] Daniel van der Lelie,[‡] and Oleg Gang*,[†]

Center for Functional Nanomaterials and Biology Department, Brookhaven National Laboratory, Upton, New York 11973

Received July 27, 2006; E-mail: ogang@bnl.gov

The ability to regulate the kinetic behavior of DNA-based nanosystems is required for emerging nanoparticle applications in sensing,[1] nanodevice assembling,[2] and gene delivery.[3] DNA-based methodology takes advantage of the tunable and programmable hybridization between DNA-capped nanomaterials.[1,3−10] This approach has allowed for the development of sensitive colorimetric detection based on the optical and physical properties of assembled nanoparticles, as well as detection based on their novel melting/disassembly propensity.[1,4−9] In addition, the scaffolding properties of DNA can be used for the programmed construction of discrete assemblies[6,7] and well-defined 2D arrays of nanoparticles with nanometer precision.[10,11] As these systems allow for more sophisticated detection and increasingly complex bottom-up construction, a protocol for the regulation of their assembly kinetics would be beneficial. This ability is especially important since single-stranded DNA is known to form highly entropic secondary structures, and its bases coordinate strongly to metal surfaces,[12] which may inhibit assembly in complex systems.

Herein, we demonstrate the tunability of assembly kinetics for DNA-capped nanoparticle systems by tailoring the conformational changes of the surface-bound DNA.[13] We used model systems of gold nanoparticles (**Au**, 9.6 ± 0.6 nm) complementary-capped with either single-stranded (ss) or partially rigid double-stranded (ds) designs, as illustrated in Scheme 1. The **Au** were encapsulated with ∼50 ssDNA of type-**1** (**1** = 5′-TAC TTC CAA TCC AAT-$(T)_{15}$-C_3H_6-SH-3′) or type-**2** (**2** = 5′-ATT GGA TTG GAA GTA-$(T)_{15}$-C_3H_6-SH-3′) forming **1-Au** and **2-Au**, respectively. In the first assembly system (**sys-I**), only ssDNA capping was used (i.e., **1-Au** + **2-Au**). In system 2 (**sys-II**), the identical **1-Au** and **2-Au** were first partially hybridized at their poly-dT spacer segment with a 15 base poly-dA strand, forming a more rigid dsDNA capping of **1*-Au** and **2*-Au** (see Supporting Information). This hybridization results in a conformational change from coiled ssDNA to partially rigid dsDNA, which causes the extension of the linker sequences away from the particle interface, helping to overcome the assembly interfering effects of coiling and base coordination to the **Au** interface.[12] A third system (**sys-III**) used an equal mixture of ssDNA and dsDNA capping (not shown). The assembly in **sys-I** and **sys-II** led to the well-documented growth of larger aggregates containing thousands of individually isolated **Au**.[4,5] The melting properties of these aggregates were characterized,[5] revealing melting temperatures (T_m) of ∼59 and ∼61 °C for **sys-I** and **sys-II**, respectively (see Supporting Information). These results provide evidence for the DNA linkages between **Au** and suggest local differences between **sys-I** and **sys-II**.

To investigate these differences, we monitored the self-assembly process in situ with the UV−visible spectrophotometry (UV−vis) method. UV−vis probes the surface plasmon (SP) resonance band, which is associated with **Au** and assembled **Au** nanostructures, and

Scheme 1. An Idealized Illustration for the Self-Assembly of Gold Nanoparticles with ssDNA Capping (**sys-I**) and Partially Rigid dsDNA capping (**sys-II**)

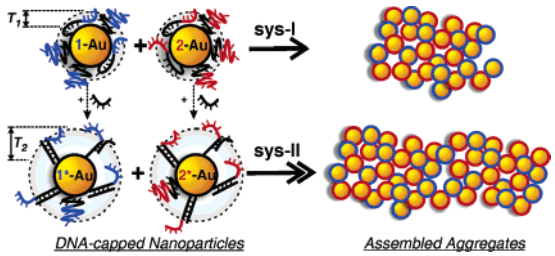

is the basis for many colorimetric detection methods.[1,4,5] Figure 1 shows a set of UV−vis data for **sys-I** (A) and **sys-II** (B), measured during assembly under identical conditions and concentrations. Assembly is apparent in the UV−vis due to a red shift in SP band position with band broadening (525−900 nm) and the decrease in extinction over time. Recently, electrodynamics simulations of the optical properties for DNA-mediated assembly revealed major contributions to the extinction spectra from the screening of **Au** within the growing aggregate, an increasing scattering component over time, and the requirement that aggregates contain a few hundred individual **Au** to show changes similar to Figure 1.[4] In the experimental system, the aggregation is also followed by sedimentation at long assembly times. For **sys-I** (Figure 1A), the first hour of assembly reveals little observable changes to the SP band (a, b). Over the course of ∼8 h, the SP band undergoes a small red shift in wavelength from 525 to 533 nm, with a noticeable extinction decrease (c, e). These changes for **sys-I** are the result of relatively inefficient hybridization between **1-Au** and **2-Au** and slow aggregate growth.

In contrast, Figure 1B shows the enhanced UV−vis progression for **sys-II**, which reveals two major differences from **sys-I**. First, there is an immediate SP band red shift to ∼535 nm (a), followed by a continued red shift and broadening after 1 h (b). Second, the decrease in extinction at long reaction times proceeds at a much higher rate (c−e). These optical changes suggest increased assembly kinetics and larger aggregate sizes in **sys-II** compared to those in **sys-I**. To investigate aggregate size and morphology, Transmission Electron Microscopy (TEM) results for samples from the corresponding UV−vis spectra are also shown in Figure 1A,B. A trend of increasing aggregate size during assembly is clearly observed, with aggregates for **sys-II** showing larger morphologies for a given assembly time. To probe the structural details of these aggregates in their native buffer environments, we utilized in situ Small-Angle X-ray Scattering (SAXS) with synchrotron radiation.[14] SAXS results revealed interparticle distances for the assembled aggregates of 11−12 nm after annealing at 50 °C, with **sys-II** consistently showing larger interparticle distances by 0.5−1.0 nm over **sys-I** (see Supporting Information).

[†] Center for Functional Nanomaterials.
[‡] Biology Department.

10.1021/ja0654229 CCC: $33.50

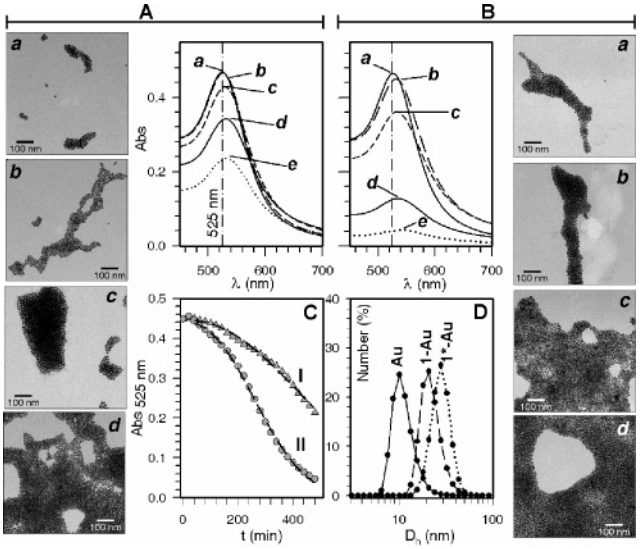

Figure 1. Representative UV−vis and TEM results for the assembly in **sys-I** (A) and **sys-II** (B) measured at 10 (a), 60 (b), 180 (c), 350 (d), and 485 (e) min. ([**1-Au**] = [**2-Au**] = 4.6 nM, [**1*-Au**] = [**2*-Au**] = 4.6 nM, 0.3 M PBS). (C) The kinetic plots for **sys-I** (**I**) and **sys-II** (**II**) as monitored by UV−vis at 525 nm with Avrami fitting (dashed line). (D) DLS results for uncapped **Au**, **1-Au**, and **1*-Au**.

To further assess the assembly process in **sys-I** and **sys-II**, we monitored kinetics by following the SP band at 525 nm (Figure 1C). The kinetic plots describe a gradual decay in absorbance, which is more prominent for **sys-II**. The kinetic profiles for additional wavelengths revealed similar trends (see Supporting Information). To qualitatively compare and contrast these kinetic profiles, we described them using Avrami law for nucleation and growth.[15] Assuming that the SP band at 525 nm is mainly attributed to the individual particles and relatively small aggregates (few hundred **Au**), an expression of Avrami law can be parametrized for the UV−vis monitoring as $\mathrm{Abs} = \mathrm{Abs}_0\exp(-((t - t_0)/\tau)^n)$, where t is assembly time, t_0 is reaction onset time, τ is the characteristic time that depends on reaction rate and aggregate geometry, and n is the Avrami exponent that depends on the physical mechanism of aggregate growth. While this description does not separate various factors that influence extinction, as described above, it provides a reasonable description of the observed effects. By fitting the kinetic plots in Figure 1C, we determined τ of 568 and 328 min and n of 2.2 and 2.4 for **sys-I** and **sys-II**, respectively. The decrease in τ for **sys-II** is indicative of an increased assembly rate, while the magnitude of n suggests a nonconstant reaction rate, which can be attributed to diffusion-limited growth and coalescence of the growing aggregates. The magnitude of τ was influenced by **Au** concentration as well as DNA surface density; however, the trend in kinetics, **sys-II** > **sys-I**, was always observed. It is interesting to note that **sys-III**, which possessed a component of both **sys-I** and **sys-II** (i.e., **1-Au** + **2*-Au**), showed an intermediate τ of 492 min (see Supporting Information).

We attribute the observed kinetic enhancement (∼2-fold) to the added rigidity of the DNA capping, which causes the extension of linker sequences away from the **Au** interface. To model this effect, we estimated the DNA-capping *thickness* (T) for the particles in each system (Scheme 1). The T for nanoparticles in **sys-I** (T_1) was modeled as $T_1 = T_1^{\mathrm{C}} \sim 6$ nm, where T_1^{C} is the end-to-end distance of a 30 base random coil oligonucleotide as described by the worm-like chain model.[13] The T for nanoparticles in **sys-II** was modeled as $T_2 = T_2^{\mathrm{R}} + T_2^{\mathrm{C}} \sim 9$ nm, where T_2^{R} is the length of the rigid dsDNA 15-bp spacer segment, and T_2^{C} is the end-to-end distance for the remaining 15 base oligonucleotide. From this approximation, we can expect a T increase of ∼3 nm for isolated nanoparticles in **sys-II** versus **sys-I**. To measure the actual changes in T, we utilized Dynamic Light Scattering (DLS). Figure 1D shows the DLS results for isolated uncapped **Au**, **1-Au**, and **1*-Au**, which revealed hydrodynamic diameter values (D_{h}) of ∼10.1, ∼21.0, and ∼28.1 nm, respectively. These values correspond to a T of ∼5.5 and ∼9.0 nm for the **1-Au** (**sys-I**) and **1*-Au** (**sys-II**). This ∼3.5 nm increase in T for the isolated nanoparticles is close to the estimated model, and taken with the SAXS results, showing an increased interparticle distance for **sys-II** for the assembled aggregates, reinforces the conclusion that the extension of linker segments from the interface is responsible for more favorable assembly conditions.

In summary, we have illustrated the approach of utilizing the conformational changes between a ssDNA and a partially dsDNA DNA capping as a method toward tuning nanoparticle assembly interactions. By increasing the rigidity of the DNA-capping structure, we allowed for the extension of crucial linker segments away from the nanoparticle interface, which facilitated enhanced assembly kinetics. This approach can be generalized for more sophisticated DNA-capped systems, which have potential use in nanoconstruction by design.

Acknowledgment. Research carried out at the Center for Functional Nanomaterials, and the National Synchrotron Light Source, was supported by the U.S. DOE Office of Science and Office of Basic Energy Sciences, under Contract No. DE-AC-02-98CH10866. M.M.M. acknowledges a Goldhaber Distinguished Fellowship at BNL sponsored by Brookhaven Science Associates. We thank Dr. H. Li, Dr. L. Zhang, and Dr. B. Panessa-Warren for assistance with TEM, and Dr. B. M. Ocko for the use of the X22b beamline at NSLS.

Supporting Information Available: Additional experimental details, melting analysis, HRTEM, UV−vis, DLS, and SAXS results. This material is available free of charge via the Internet at http://pubs.acs.org.

References

(1) Rosi, N. L.; Mirkin, C. A. *Chem. Rev.* **2005**, *105*, 1547−1562.
(2) (a) Rothemund, P. W. K. *Nature* **2006**, *440*, 297−302. (b) Seeman, N. C.; Lukeman, P. S. *Rep. Prog. Phys.* **2005**, *68*, 237−270.
(3) Rosi, N. L.; Giljohann, D. A.; Thaxton, C. S.; Lytton-Jean, A. K. R.; Han, M. S.; Mirkin, C. A. *Science* **2006**, *312*, 1027−1030.
(4) (a) Storhoff, J. J.; Lazarides, A. A.; Mucic, R. C.; Mirkin, C. A.; Letsinger, R. L.; Schatz, G. C. *J. Am. Chem. Soc.* **2000**, *122*, 4640−4650. (b) Lazarides, A. A.; Schatz, G. C. *J. Phys. Chem. B* **2000**, *104*, 460−467.
(5) Jin, R.; Wu, G.; Li, Z.; Mirkin, C. A.; Schatz, G. C. *J. Am. Chem. Soc.* **2003**, *125*, 1643−1654.
(6) Claridge, S. A.; Goh, S. L.; Fréchet, J. M. J.; Williams, S. C.; Micheel, C. M.; Alivisatos, A. P. *Chem. Mater.* **2005**, *17*, 1628−1635.
(7) Zanchet, D.; Micheel, C. M.; Parak, W. J.; Gerion, D.; Alivisatos, A. P. *Nano Lett.* **2001**, *1*, 32−35.
(8) Hazarika, P.; Ceyhan, B.; Niemeyer, C. M. *Angew. Chem., Int. Ed.* **2004**, *43*, 6469−6471.
(9) Dillenback, L. M.; Goodrich, G. P.; Keating, C. D. *Nano Lett.* **2006**, *6*, 16−23.
(10) Zhang, J.; Liu, Y.; Ke, Y.; Yan, H. *Nano Lett.* **2006**, *6*, 248−251.
(11) Pinto, Y. Y.; Le, J. D.; Seeman, N. C.; Musier-Forsyth, K.; Taton, T. A.; Kiehl, R. A. *Nano Lett.* **2005**, *5*, 2399−2402.
(12) (a) Östblom, M.; Liedberg, B.; Demers, L. M.; Mirkin, C. A. *J. Phys. Chem. B* **2005**, *109*, 15150−15160. (b) Storhoff, J. J.; Elghanian, R.; Mirkin, C. A.; Letsinger, R. L. *Langmuir* **2002**, *18*, 6666−6670. (c) Parak, W. J.; Pellegrino, T.; Micheel, C. M.; Gerion, D.; Williams, S. C.; Alivisatos, A. P. *Nano Lett.* **2003**, *3*, 33−36.
(13) (a) Rubinstein, M.; Colby, R. H. *Polymer Physics*; Oxford University Press: New York, 2003. (b) Rivetti, C.; Walker, C.; Bustamante, C. *J. Mol. Biol.* **1998**, *280*, 41−59.
(14) Park, S.-J.; Lazarides, A. A.; Storhoff, J. J.; Pesce, L.; Mirkin, C. A. *J. Phys. Chem. B* **2004**, *108*, 12375−12380.
(15) (a) Avrami, M. J. *Chem. Phys.* **1940**, *8*, 212−240. (b) Rikvold, P. A.; Tomita, H.; Miyashita, S.; Sides, S. W. *Phys. Rev. E* **1994**, *49*, 5080−5090.

JA0654229